

Asymmetries in the CMB anisotropy field

Hans K. Eriksen¹

*Institute of Theoretical Astrophysics, University of Oslo, P.O. Box 1029 Blindern,
N-0315 Oslo, Norway*

h.k.k.eriksen@astro.uio.no

Frode K. Hansen

*Dipartimento di Fisica, Università di Roma ‘Tor Vergata’, Via della Ricerca Scientifica 1,
I-00133 Roma, Italy*

Anthony J. Banday

*Max-Planck-Institut für Astrophysik, Karl-Schwarzschild-Str. 1, Postfach 1317,
D-85741 Garching bei München, Germany*

Krzysztof M. Górski²

JPL, M/S 169/327, 4800 Oak Grove Drive, Pasadena CA 91109

and

Per B. Lilje¹

*Institute of Theoretical Astrophysics, University of Oslo, P.O. Box 1029 Blindern,
N-0315 Oslo, Norway*

ABSTRACT

We report on the results from two independent but complementary statistical analyses of the WMAP data. In the first, the data are subjected to an N -point correlation function analysis, and in the second to a power spectrum analysis. We focus on large and intermediate scales (larger than about 3°), and compare the observed data on these scales against Monte Carlo ensembles with WMAP-like

¹Also at Centre of Mathematics for Applications, University of Oslo, P.O. Box 1053 Blindern, N-0316 Oslo, Norway

²Also at Warsaw University Observatory, Aleje Ujazdowskie 4, 00-478 Warszawa, Poland

properties. On the largest scales we find that the WMAP data contain too little structure overall; both the two-point and three-point correlation functions reject the model at the 3σ level. Even more importantly, we find clear asymmetries between pairs of hemispheres. The northern and western galactic hemispheres and the northern ecliptic hemisphere have much less large scale fluctuations than the simulated maps, whereas the southern and eastern galactic hemispheres and the southern ecliptic hemisphere show relatively stronger fluctuations. The same asymmetries are also found on intermediate scales, as measured by correlation functions at $3\text{--}5^\circ$. Also, comparison of the hemisphere power spectra yields consistent results; the ratio of the northern to the southern ecliptic hemisphere power spectrum is found to be low in the multipole range $\ell \approx 2\text{--}35$ at the 3σ confidence level. Finally, in order to check for systematics, we study the power spectra also from the *COBE*-DMR maps, and find similar asymmetries in those data.

Subject headings: cosmic microwave background — cosmology: observations — methods: statistical

1. Introduction

In recent months much interest has focused on the question of lack of large-scale power in the WMAP³ (Bennett et al. 2003a) data sets (e.g., Efstathiou 2003a, b; Spergel et al. 2003; Tegmark, de Oliveira-Costa, & Hamilton 2003). In this Letter we present new evidence for this effect, although we do not restrict our analysis to the very largest scales. Our tests indicate that there are significant effects also on slightly smaller scales, down to $3\text{--}5^\circ$. In particular, the lack of large-scale power is not uniformly distributed over the full-sky; the effect is significantly more prominent on the northern than on the southern galactic (and ecliptic) hemisphere.

This Letter is organized as follows: In §2 we give a brief review of the statistical tests under consideration, before reporting on the results in §3. Finally, we conclude with a discussion on the significance of our findings. Thorough reports from these analyses will be published shortly by Hansen et al. (2003, in preparation) and Eriksen et al. (2003, in preparation). Similar results based on genus statistics were very recently reported by Park (2003). Thus, at the moment three qualitatively different methods find consistent results.

³Wilkinson Microwave Anisotropy Probe

2. Definitions

In this Letter we analyze the WMAP data both by means of the angular power spectrum (using both the Gabor transform method [Hansen, Górska, & Hivon 2002] and the MASTER method [Hivon et al. 2003]), and its real-space complements, the N -point correlation functions [e.g., Eriksen, Banday, & Górska 2002]). While we do not aim at presenting the full statistical machinery behind these methods here, we will give a brief overview of each method, and refer to the upcoming papers for details.

2.1. N -point correlation functions

An N -point correlation function is the average product of N temperatures, as measured in a fixed relative orientation on the sky,

$$C_N(\theta_1, \dots, \theta_{2N-3}) = \left\langle \Delta T(\hat{n}_1) \cdots \Delta T(\hat{n}_N) \right\rangle, \quad (1)$$

where the unit vectors $\hat{n}_1, \dots, \hat{n}_N$ span an N -point polygon on the sky. Algorithmically speaking, these functions are estimated as simple averages,

$$C_N(\theta_1, \dots, \theta_{2N-3}) = \frac{\sum_i w_1^i \cdots w_N^i \cdot T_1^i \cdots T_N^i}{\sum_i w_1^i \cdots w_N^i}. \quad (2)$$

Here the sums go over all sets of N pixels fulfilling the geometric requirements set by $\theta_1, \dots, \theta_{2N-3}$. The weights, w_i , may be independently chosen for each pixel in order to reduce, e.g., noise or border effects. In this Letter we let these weights represent masking, and define them to be 1 for included pixels and 0 for excluded pixels.

The degree of agreement between the simulations and the observations is quantified in terms of the covariance matrix χ^2 statistic described by Eriksen et al. (2003, in preparation).

2.2. The angular power spectrum

The angular power spectrum is defined through the spherical harmonic coefficients, $a_{\ell m}$, of the CMB temperature field,

$$C_\ell = \sum_{m=-\ell}^{\ell} \frac{a_{\ell m} a_{\ell m}^*}{2\ell + 1}.$$

The power spectrum can be estimated on a given patch on the sky using a maximum-likelihood approach with the observed, cut-sky power spectrum \tilde{C}_ℓ (called the pseudo power

spectrum) as the input data (Hansen et al. 2002). One can also obtain the power spectrum using the quadratic statistic

$$C_\ell = \sum_{\ell'} K_{\ell\ell'} (\tilde{C}_{\ell'} - \tilde{N}_{\ell'}),$$

where \tilde{N}_ℓ is the noise power spectrum on the given patch and $K_{\ell\ell'}$ is the kernel connecting the full sky and cut sky power spectrum. Both these methods are used in this Letter.

Histograms of the estimated C_ℓ from the simulations are used to quantify the percentage level of agreement between simulations and the real sky measurements.

3. Results

3.1. Preparation of the data

The analyses are carried out by means of Monte Carlo simulations: we simulate an ensemble of stochastic realizations based on WMAP-like properties, and compare the observed data with our simulations through the different statistics.

Our simulations are based on the WMAP running-index spectrum⁴, a choice which is based on the fact that this spectrum has less power on large scales than the power law spectrum, and therefore should provide a better fit to the WMAP results in our scale range, knowing *a priori* that the WMAP data have little power on these scales. However, a number of tests were also run with the power law spectrum, and similar results were found there. The details of the simulation process is described by e.g., Hinshaw et al. (2003), and we use the template method of Bennett et al. (2003b) to correct for foregrounds. The correlation function tests are calibrated against ensembles of 5000 realizations, whereas the power spectrum tests are compared against 768 Monte Carlo realizations.

Next, the N -point correlation functions are computed from low-resolution, $N_{\text{side}} = 64$, maps, which are made by first de-convolving the old beam and pixel windows from each band, and then convolving with a Gaussian beam of FWHM=140' and an $N_{\text{side}} = 64$ pixel window. Finally the maps are co-added using the same inverse-noise weights as used for generating the $N_{\text{side}} = 512$ maps.

For the power spectra tests we use the Kp2 mask, while for the N -point functions we use the Kp0 mask. However, since we in the latter case smooth all maps with a relatively wide Gaussian beam, also the foregrounds are smoothed out. For this reason we extend the mask

⁴available at <http://lambda.gsfc.nasa.gov>

itself by one FWHM in all directions before proceeding. The power spectra are calculated from the weighted, co-added $V + W$ WMAP maps of $N_{\text{side}} = 512$, with the effective noise and beam properties of the co-added $V + W$ WMAP maps.

3.2. N -point correlation function results

The correlation function analyses are designed to probe two different ranges of scales: First, the very largest scales are analyzed by measuring the correlation functions from the full sky, covering scales over the full range between 0 and 180° , in a total of 180 two-point bins and 120 three-point configurations. The same functions are also computed from six different hemispheres, namely the north, south, east and west galactic hemispheres, and the north and south ecliptic hemispheres.

Second, scales between 3 and 5° are probed by partitioning the sphere into 81 disks, each of 10° radius, and computing the three-point correlation function on each of these. In order to reduce disk-disk correlations we first apply a high-pass filter to the maps, removing all multipoles with $\ell = 0, \dots, 18$ (details are given by Eriksen et al. [2003, in preparation]). On each of these disks we compute the three-point correlation functions for 460 isosceles configurations smaller than 5° .

In Figure 1, the two-point and equilateral three-point functions are shown as computed on the northern and southern galactic hemispheres (note that the angular scales are different in the upper and lower panels). As has been reported by several authors (e.g., Bennett et al. 2003a), the full-sky two-point correlation function is practically zero at angles larger than 60° . However, as we can see from the upper panel of Figure 1, this is primarily because of the (absence of) contributions from the northern hemisphere: the southern hemisphere two-point function is visually quite acceptable, following the overall shape of the confidence regions very well. The northern hemisphere two-point function is clearly not.

This difference is even clearer for the three-point correlation function, since we in this case compare the function value against zero, rather than an average that itself varies: the northern hemisphere three-point correlation function shows a spectacular lack of fluctuations, whereas the southern hemisphere function appears to be acceptable.

In order to quantify these statements, we use the full covariance matrix χ^2 statistic, which both measures the overall level of deviation, but also, and even more importantly, bin-to-bin correlations. The results from these computations are shown in Table 1. As we see, the two-point correlation function is rejected by more than 3σ on the full sky and on the northern and eastern galactic hemispheres, and more than 2.5σ on the other hemispheres.

However, the two-point function is a sub-optimal discriminator for this effect, since it is compared against a non-zero average. Thus, the variation in the average itself is interpreted as a variation of the observed two-point function by the χ^2 statistic, and the “flatness” is not properly accounted for.

This is not the case with the three-point function which has a vanishing mean. And in this case the lack of large-scale power is striking: *no* single realization has a lower χ^2 than that measured on the northern and eastern galactic hemispheres and on the northern ecliptic hemisphere. In comparison the complementary hemispheres are comfortably accepted by the three-point function.

The top panel of Figure 2 shows the smoothed, co-added WMAP map, and in this Figure it is possible to see the asymmetry by eye; while there is a fair amount of large-scale features visible on the southern hemisphere, the northern hemisphere is surprisingly featureless.

In order to localize these features further, we show the three-point correlation functions on a set of 81 disks in the middle panel of Figure 2. There is clearly an asymmetry also on these scales; large connected regions on the northern hemisphere have a low χ^2 , whereas the southern hemisphere (especially the eastern quadrant) has a higher χ^2 . There can possibly be seen an alignment with the ecliptic poles, in agreement with the results from the hemisphere measurements.

3.3. Power spectrum results

The power spectra are estimated both on the full sky and on the northern and southern ecliptic hemispheres separately, using the quadratic estimator. We have also computed the power spectra on the northern and southern galactic hemispheres, and for the eastern and western galactic hemispheres (the western galactic hemisphere is defined as the hemisphere where $l < 180^\circ$, which is the left half of the projected maps in Figure 2).

In Figure 3, the full sky power spectrum (downloaded from the WMAP web site) is shown as a grey dashed line and the best-fit spectrum (running-index) as a solid line histogram. The 1σ and 2σ confidence levels are marked as light and dark grey bands, respectively. The black crosses (northern) and grey dots (southern) are the spectra estimated on each ecliptic hemisphere separately.

We see that the number of bins of the estimated northern and southern spectra outside the 1 and 2σ bands is as expected, assuming the theoretical spectrum to be correct. Note however that whereas the southern spectrum tends to have higher amplitude than the theo-

retical spectrum (with an average value of about $1100 \mu\text{K}$), the northern spectrum tends to have lower amplitude than both the theoretical spectrum and the southern spectrum up to $\ell \approx 35$ (average value of about $900 \mu\text{K}$). Yet, the difference between the two spectra is not striking, and the asymmetry is certainly not localized to one or a few multipoles.

For the same three pairs of hemispheres for which we computed the correlation functions, we have also determined the power spectra. The spectra are computed in four different bins from $\ell = 2\text{--}34$ to $\ell = 11\text{--}34$, i.e., having different lower limits, and are presented in Table 2. In the Table the numbers denote the fraction of simulated maps with a lower value than that of the observed map under consideration. The Table seems to indicate a strong asymmetry present in all three pairs of hemispheres, both with and without the lowest multipoles ($\ell < 10$) included. Further tests with alternative theoretical power spectra show that this effect is not sensitive to the underlying model.

The same exercise has been performed for the co-added 53+90 GHz *COBE*-DMR map (using only the pseudo spectra from each hemisphere, corrected for noise). For the $\ell = 5\text{--}20$ bin, we find similar asymmetries, showing that this kind of features is not only confined to the WMAP data.

To further localize the effect, we perform a power spectrum estimation of the bin $\ell = 2\text{--}32$ (and $\ell = 11\text{--}34$, with identical results) on hemispheres centered on 164 different positions on the sphere. Once again we calculate the ratio between the first bin value of the opposite pairs of hemispheres, and the results from these computations are shown in the bottom panel of Figure 2. The ratio of the bin value of the two hemispheres is indicated by the color of the large disks, where the disk itself represents the north pole of the current hemispheres. Light red/yellow indicates a low ratio whereas dark red indicates a high ratio. The positions of the ecliptic poles are marked by the two medium-sized dark blue spots. A very similar pattern is again found when subjecting the *COBE*-DMR data to the same analysis.

The power spectra are finally estimated on 164 slightly overlapping 9.5° radius disks (which above served as the *centers* of the hemispheres), using the likelihood approach (i.e., the Gabor transforms). The power spectrum bin under consideration is in this case defined to be $\ell = 2\text{--}63$. Also the results from this experiment are shown in the bottom panel of Figure 2, by small dots at the centers of each disk. A green dot indicates that the power spectrum value computed from the corresponding disk lies *above* the *upper* 1σ region, while a dark blue spot means that it lies *below* the *lower* 1σ region. Note how well this figure corresponds to the map showing the three-point correlation function results: low values are found on the western half of the northern galactic hemisphere, while high values are found on the eastern half of the southern galactic hemisphere. Thus, also this figure suggests that the direction of peak asymmetry is aligned with (but not directly on) the ecliptic poles.

4. Conclusions

In this Letter we have estimated power spectra and N -point correlation functions from the WMAP data, and compared these against Monte Carlo ensembles based on realizations of a Gaussian process with the global WMAP best-fit running-index power spectrum. We found that the previously reported lack of large scale power in WMAP is highly significant, and, perhaps more importantly, that this lack of power is non-uniformly distributed on the sky. Specifically, the northern galactic (and ecliptic) hemisphere is practically devoid of large-scale power, while the southern hemisphere shows a much better agreement with the model. The missing large-scale power on the northern hemisphere is clearly demonstrated by the correlation functions; *no* simulation out of 5000 shows such a strikingly featureless three-point function as that computed from the WMAP northern galactic hemisphere.

Also, computing the angular power spectrum separately for the northern and southern ecliptic hemispheres, we found that while the lowest multipoles ($\ell \approx 2\text{--}35$) seem to lack power compared to the model on the northern hemisphere, too much power is present on the southern hemisphere. Further, we found that the ratio between the ecliptic northern and southern spectra for WMAP is too low at the 3σ confidence level, as compared to an ensemble of 768 simulated realizations. We also found that this asymmetry is present even when considering a higher multipole range like $\ell \approx 10\text{--}35$, consistent with the findings of the intermediate scale correlation functions. Similar asymmetries are also found between the northern and southern hemispheres, and between the eastern and western galactic hemispheres.

As a check on systematic effects, we have estimated the power spectra also from the *COBE*-DMR data, and found that similar asymmetries are present in that data set. We have also computed the correlation functions from each of the three cosmologically interesting frequency bands (not reported here), and found equivalent results in each band.

In order to localize these effects further we computed the correlation functions and power spectra on small disks uniformly distributed on the sphere, and we found that the location of peak asymmetry is roughly consistent between the power spectrum and correlation function results, both preferring a direction close to, but not directly on, the ecliptic poles.

These observations will be discussed in more detail in two upcoming papers (Hansen et al. 2003, in preparation; Eriksen et al. 2003, in preparation).

FKH acknowledges financial support from the CMBNET Research Training Network and FKH and PBL acknowledges financial support from the Research Council of Norway. We acknowledge use of the HEALPix (Górski et al. 1998) software and analysis package for deriving the results in this Letter. This research used resources of the National Energy

Research Scientific Computing Center, which is supported by the Office of Science of the U.S. Department of Energy under Contract No. DE-AC03-76SF00098. This work has also received support from The Research Council of Norway (Programme for Supercomputing) through a grant of computing time.

REFERENCES

Bennett, C. C., et al. 2003a, ApJ, in press (astro-ph/0302207)

Bennett, C. C., et al. 2003b, ApJ, in press (astro-ph/0302208)

Efstathiou, G. 2003a, MNRAS, in press (astro-ph/0303127)

Efstathiou, G. 2003b, preprint (astro-ph/0306431)

Eriksen, H. K., Banday, A. J. & Górski, K. M. 2002, A&A, 395, 409

Górski, K. M., Hivon, E., & Wandelt, B. D. 1998, in ‘Analysis Issues for Large CMB Data Sets’, eds A. J. Banday, R. K. Sheth and L. Da Costa, ESO, Printpartners Ipskamp, NL, pp. 37–42 (astro-ph/9812350); Healpix homepage: <http://www.eso.org/science/healpix/>

Hansen, F. K., Górski, K. M., & Hivon, E. 2002, MNRAS, 336, 1304

Hinshaw, G., et al. 2003, ApJ, in press (astro-ph/0302217)

Hivon, E., Górski, K. M., Netterfield, C. B., Crill, B. P., Prunet, S., & Hansen, F. K. 2002, ApJ, 567, 2

Park, C.-G. 2003, preprint (astro-ph/0307469)

Spergel, D. N., et al. 2003, ApJ, in press (astro-ph/0302209)

Tegmark, M., de Oliveira-Costa, A., & Hamilton, A. 2003, preprint (astro-ph/0302496)

Table 1. N -point correlation function χ^2 results

Function	Galactic		Galactic		Ecliptic		
	North	South	West	East	North	South	Full sky
Two-point function	0.996	0.988	0.999	0.996	1.000	0.995	0.999
Three-point function	0.000	0.136	0.000	0.084	0.000	0.276	0.000

Note. — Results from χ^2 tests of the large scale correlation functions. The numbers indicate the fraction of simulated realizations with a χ^2 value *lower* than for the co-added WMAP map. The values 0.000 and 1.000 are reserved for the cases in which respectively no or all simulations have a lower χ^2 value.

Table 2. Power spectrum results

Data set	Galactic			Galactic			Ecliptic		
	North	South	Ratio	West	East	Ratio	North	South	Ratio
WMAP, $\ell = 2 - 34$	0.197	0.977	0.026	0.104	0.957	0.014	0.034	0.987	0.003
WMAP, $\ell = 5 - 34$	0.173	0.980	0.024	0.138	0.928	0.033	0.055	0.984	0.004
WMAP, $\ell = 9 - 34$	0.089	0.948	0.021	0.137	0.924	0.042	0.057	0.992	0.007
WMAP, $\ell = 11 - 34$	0.187	0.836	0.091	0.268	0.932	0.058	0.099	0.965	0.017
DMR, $\ell = 5 - 20$	0.058	0.034	0.137

Note. — The value of the first power spectrum bin computed from the WMAP and *COBE*-DMR maps, as compared to 768 simulated realizations. The numbers indicate the fraction of simulations with lower value than that indicated by the column header.

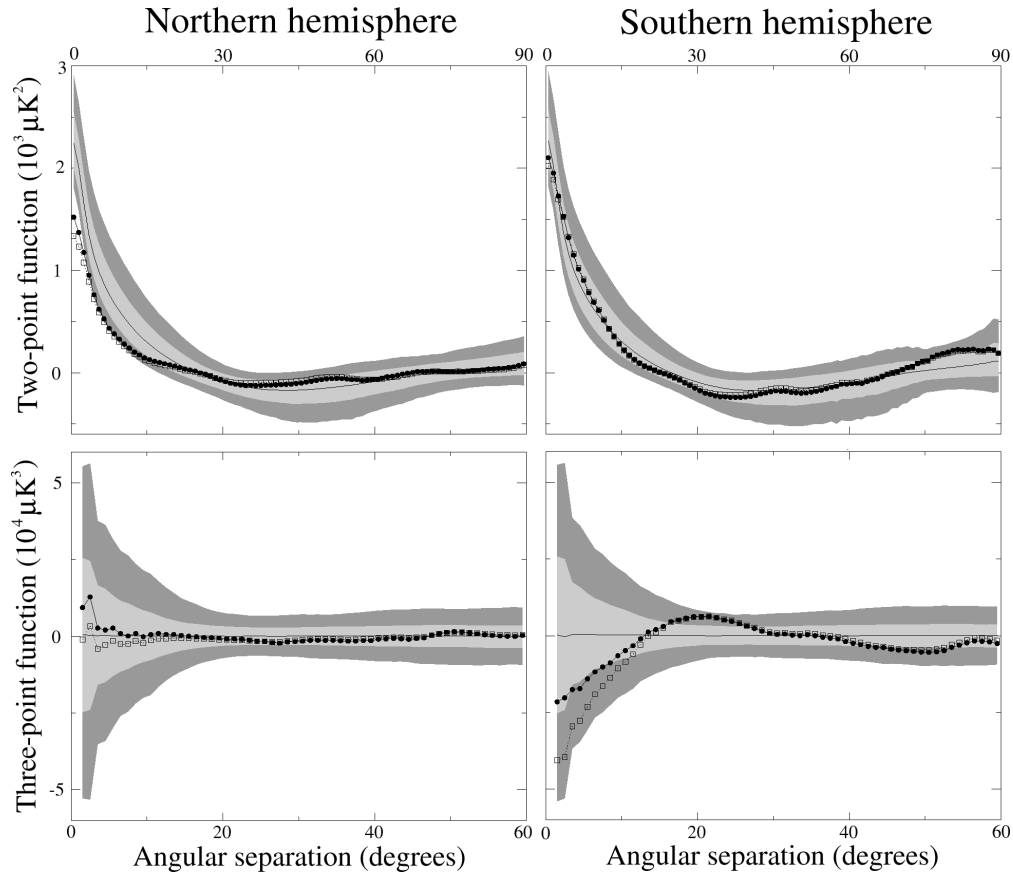


Fig. 1.— The two- and three-point correlation functions as computed from the low-resolution co-added WMAP map. The grey bands indicate 1σ and 2σ confidence regions as computed from a set of 5000 Monte Carlo simulations. Filled dots show the raw co-added WMAP map, and boxes show the foreground corrected, co-added WMAP map. Note that the angular scales are different for the two- and three-point correlation functions.

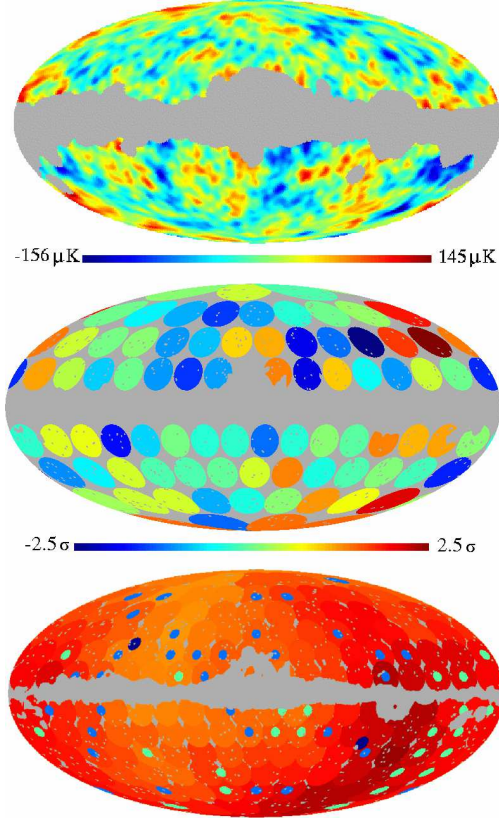


Fig. 2.— Top panel: The low-resolution co-added WMAP map. Middle panel: The results from the intermediate scale three-point analysis. Blue corresponds to low χ^2 , which again corresponds to small fluctuations in the three-point function, while red corresponds to high χ^2 . Bottom panel: Results from power spectrum analysis. The color of the 9.5° disks indicate the ratio between the $\ell = 2\text{--}64$ power spectrum bin of the northern and southern hemispheres, where the disk itself defines the north pole of the coordinate system; light red/yellow indicates a low ratio, dark red a large ratio. The small dots in the disk centers indicate the absolute value of the power spectrum estimated on that disk in the $\ell = 2\text{--}64$ bin (i.e., not on the full hemisphere), and a dark blue dot means that this value lies *below* the *lower* 1σ confidence limit, while a green dot means it lies *above* the *upper* 1σ limit. Finally, the ecliptic poles are marked by the medium sized dark blue spots.

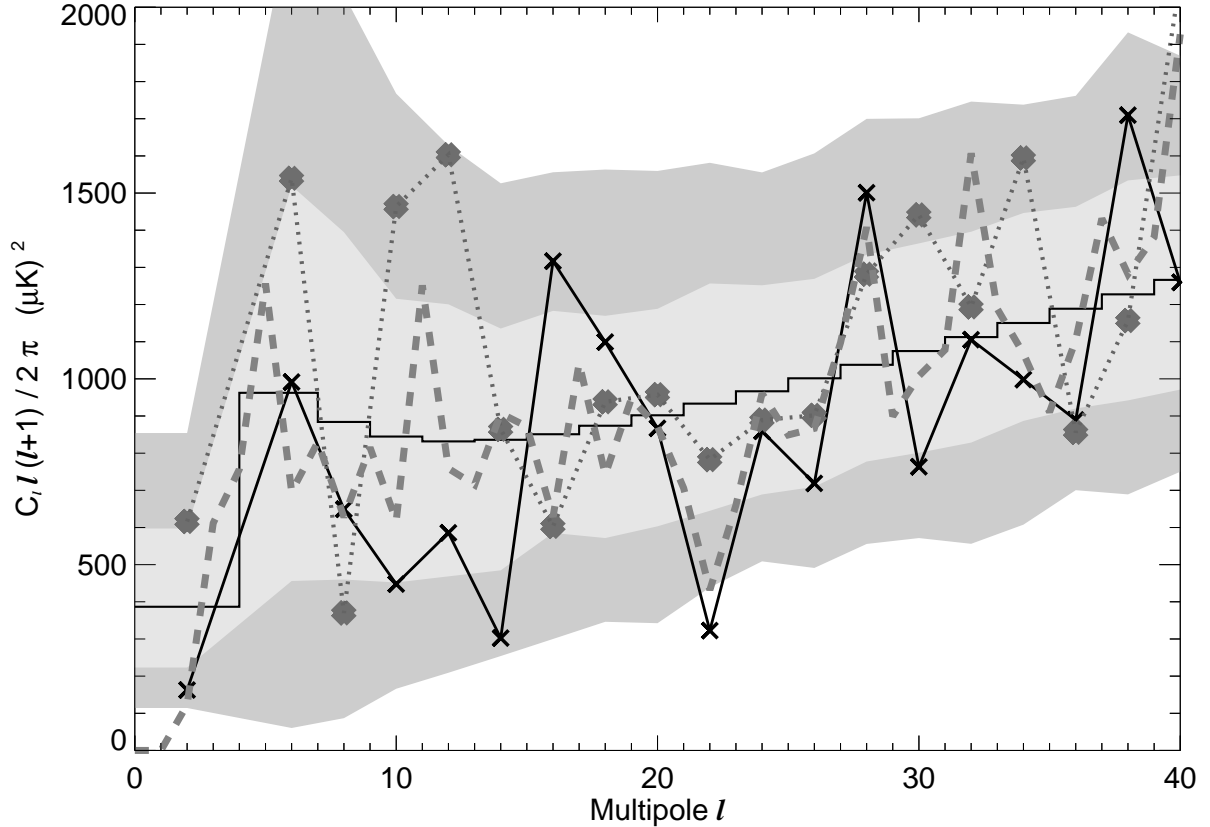


Fig. 3.— The power spectra as computed from different regions on the sky. The solid line (histogram) indicates the theoretical best-fit WMAP running index power spectrum (available at the WMAP web site), whereas the dashed line shows the estimated power spectrum obtained by the WMAP team. The black crosses and grey dots, respectively, are our estimates of the power spectra on the northern and southern ecliptic hemispheres. The grey bands indicate the 1σ and 2σ confidence regions, as computed from the ensemble of 768 Monte-Carlo simulations.